

# Jet quenching by (pre-)hadronic final state interactions at RHIC

K. Gallmeister<sup>a,\*</sup> W. Cassing<sup>a</sup>

<sup>a</sup>*Institut für Theoretische Physik, Universität Giessen, Heinrich-Buff-Ring 16,  
D-35392 Giessen, Germany*

---

## Abstract

Within a hadron-string dynamical transport approach (HSD) we investigate the attenuation of high transverse momentum ( $p_\perp$ ) hadrons as well as the suppression of 'near-side' and 'far-side' jets in  $Au + Au$  collisions at invariant energies  $\sqrt{s} = 200$  GeV and  $\sqrt{s} = 62.4$  GeV in comparison to the data available from the Relativistic Heavy-Ion Collider (RHIC). From our transport studies we find that a significant part of the high  $p_\perp$  hadron attenuation seen experimentally can be attributed to inelastic interactions of 'leading' pre-hadrons with the dense hadronic environment. In addition, we also show results of 'near-side' and 'far-side' angular correlations of high  $p_\perp$  particles from  $Au + Au$  collisions at  $\sqrt{s} = 200$  GeV and  $\sqrt{s} = 62.4$  GeV within this (pre-)hadronic attenuation scenario. It turns out that the 'near-side' correlations are unaltered – in accordance with experiment – whereas the 'far-side' correlations are suppressed by up to  $\sim 60\%$  in central collisions. Since a much larger suppression is observed experimentally for these reactions in central reactions we conclude that there should be strong additional (and earlier) partonic interactions in the dense and possibly colored medium created in  $Au + Au$  collisions at RHIC.

*Key words:* Relativistic heavy-ion collisions, Meson production, Quark-gluon plasma, Fragmentation into hadrons

*PACS:* 25.75.-q, 13.60.Le, 12.38.Mh, 13.87.Fh

---

## 1 Introduction

The phase transition from partonic degrees of freedom (quarks and gluons) to interacting hadrons is a central topic of modern high-energy physics. In order

---

\* corresponding author

*Email address:* Kai.Gallmeister@theo.physik.uni-giessen.de  
(K. Gallmeister).

to understand the dynamics and relevant scales of this transition – as well the dynamical formation of hadrons – laboratory experiments are presently performed with ultra-relativistic nucleus–nucleus collisions. Estimates based on the Bjorken formula [1] and/or calculations within hadron-string-dynamical transport approaches [2,3,4] indicate that the critical energy density for the formation of a quark–gluon plasma (QGP) of 0.7 to 1 GeV/fm<sup>3</sup> [5] should by far be exceeded in the initial phase of central Au+Au collisions for a couple of fm/c at top SPS and RHIC energies [6]. However, the task still remains to unambiguously identify the formation and properties of this new phase.

Whereas there are a couple of tentative signatures for an early partonic phase such as the high transverse pressure seen experimentally [7,8] as well as the large elliptic flow of hadrons at moderate and high momenta [7,9], a unique 'smoking gun' could not be identified so far. In order to find representative signatures one has to look for early 'hard' probes that dominantly test the first few fm/c of the relativistic heavy-ion collision. Hence, the measurements of 'hard' jets should offer a direct access to the dynamics in the early stage when the (possibly deconfined) matter is very dense. In fact, the PHENIX [10] and STAR [11] collaborations have reported a large relative suppression of hadron spectra for transverse momenta  $p_{\perp}$  above  $\sim 3\text{--}4$  GeV/c which might point towards the creation of a QGP, since this suppression is not observed in d+Au interactions at the same bombarding energy per nucleon [12,13,14] and thus has to be attributed to final state interactions. Furthermore, an almost complete suppression of 'far-side' jets has been reported for central Au+Au collisions [16] which is also not seen in d+Au reactions [17].

These observations – at first sight – appear to be compatible with the picture of partonic energy loss in a dense colored medium [18,19,20,21,22,23,24,25,26,27,28,29,30,31], however, it is not clear presently to which extent these suppression phenomena might be due to ordinary hadronic final-state-interactions (FSI) [32] since (in-)elastic collisions of (pre-)hadronic high momentum states with the bulk of hadrons in the late fireball might also contribute significantly to the attenuation of the high transverse momentum hadrons at RHIC [33,34,35]. Hence, the hadronic attenuation has to be addressed in more detail before conclusions on perturbative QCD effects in a deconfined QGP phase on the materializing jets can be drawn. In fact, as shown in Refs. [35,36] a major fraction of the high  $p_{\perp}$  hadron attenuation in Au+Au collisions at  $\sqrt{s} = 200$  GeV can be described by the (dominantly) inelastic interactions of 'leading' pre-hadrons.

In order to specify the latter findings in Refs. [35,36] we briefly recall the concept of 'leading' (pre-hadronic) and 'secondary' (ordinary) hadrons in the string-hadron transport approach: In a high energy nucleon-nucleon collision two (or more) color-neutral strings are assumed to be formed; the string ends are defined by the space-time coordinates of the constituents which are denoted as 'leading' quarks. The latter are initially colored but assumed to pick up

almost instantly a quark (or antiquark) from the vacuum to build up color neutral 'leading' pre-hadrons [37]. These pre-hadronic states are distinguished from 'secondary' hadrons that arise from the further fragmentation of the strings and consist solely of quarks and antiquarks (diquarks and antidiquarks) created from the vacuum at some later time. The total time that is needed for the fragmentation of the strings and for the hadronization of the fragments is denoted as *formation time* and taken as  $\tau_f \approx 0.8$  fm in the HSD transport approach. Due to time dilatation the formation time  $t_f$  in any reference frame is then proportional to the Lorentz  $\gamma$ -factor,

$$t_f = \gamma \tau_f. \quad (1)$$

We stress that the formation time is a sensible parameter and has been fixed in [38] by the rapidity distribution of charged particles at SPS energies in the range 0.6–0.8 fm/c. Though  $\tau_f$  is no longer a free parameter we will perform also calculations for the jet suppression in Section 4 for different  $\tau_f$  ranging from 0.2 to 0.5 fm/c. In principle, other scenarios for modeling the string fragmentation might also be investigated, e.g. formation times depending explicitly on the hadron species or those extracted from the LUND fragmentation scheme (cf. Ref. [39]); however, we here constrain to the simple model introduced in Ref. [38] and delay an investigation of alternative prescriptions to future studies.

In the HSD transport approach, furthermore, it is assumed that hadrons, whose constituent quarks and antiquarks are created from the vacuum in the string fragmentation, do *not interact* with the surrounding nuclear medium within their formation time  $t_f$  and thus do *not* create early pressure. On the other hand, for the leading pre-hadrons, i.e. those involving quarks (antiquarks) from the struck nucleons, a reduced effective cross section  $\sigma_{lead}$  is adopted during the formation time  $t_f$  and the full hadronic cross section later on. The effective cross section  $\sigma_{lead}$  is fixed in line with the additive constituent quark model [35] (cf. also Section 3).

As shown in Ref. [35] for central Au+Au collisions at  $\sqrt{s} = 200$  GeV hadrons with transverse momenta larger than  $\sim 6$  GeV/c predominantly stem from the string ends and therefore can, in principle, interact directly with the reduced cross section  $\sigma_{lead}$ . Moreover, we have to stress that in the HSD approach the formation of secondary hadrons (e.g. in Au+Au collisions) is not only controlled by the formation time  $\tau_f$ , but also by the energy density in the local rest frame: hadrons are not allowed to be formed if the energy density is larger than  $1 \text{ GeV/fm}^3$ , which is about the critical energy density for a phase transition to the QGP in thermal equilibrium [5]. The interaction of the leading and energetic (pre-)hadrons with the soft hadronic and bulk matter is thus explicitly modeled to happen only for local energy densities below that cut, i.e. pre-hadronic interactions with fully formed hadrons as well as

interactions between formed hadrons are delayed until the energy density has dropped below  $1 \text{ GeV/fm}^3$  in the expansion phase! Note, however, that the highest energy densities are achieved in the center of the 'fireball' and that the formation of hadrons starts at the surface where substantially lower energy densities are encountered.

We recall that the interactions of leading (pre-)hadrons are also important to understand the attenuation of hadrons with high (longitudinal) momentum in ordinary 'cold' nuclear matter. The studies in Refs. [39,40] (see also [41]) have shown that the dominant final-state-interactions of the hadrons with maximum momentum – as measured by the HERMES Collaboration [42] – are compatible with the concepts described above. These independent investigations impose severe constraints on hadron attenuation in a medium that might possibly be attributed to a QGP phase (cf. also Ref. [29]).

In this work we concentrate on the transverse momentum dynamics and especially on the very high momentum tail of the hadron spectra. In order to describe these high  $p_\perp$  spectra, we use the PYTHIA v6.2 event generator [43] for nucleon–nucleon collisions and the HSD transport model [38,44,45] for the space-time localization of the events and further propagation in time including final-state interactions (cf. Refs. [35,36]).

Our study is organized as follows: We start in Section 2 with an analysis of high  $p_\perp$  hadron events from  $pp$  reactions – generated via PYTHIA v6.2 – with respect to correlations in the azimuthal angle  $\varphi$  employing different momentum cuts for the hadrons. Section 3 gives a very brief reminder of the HSD approach and the actual 'input' to the transport calculations. The calculated results for jet quenching in Au+Au collisions at  $\sqrt{s} = 200 \text{ GeV}$  for different centrality classes are presented in Section 4. The sensitivity of the jet suppression to the formation time  $\tau_f$  will be demonstrated, too. In Section 5 we will show the results of calculations for Au+Au collisions at  $\sqrt{s} = 62.4 \text{ GeV}$  for different centrality classes since this system is presently under investigation experimentally. Apart from a comparison of the high  $p_\perp$  attenuation of charged hadrons with the data from the PHOBOS collaboration [46] we will also present our predictions for the 'near-side' and 'far-side' angular correlations at this energy. Section 6 summarizes our present investigations.

## 2 Jet correlations in $pp$ reactions

Before coming to the more subtle issue of jet quenching in Au+Au collisions at RHIC energies, it is instructive to have a look at the jet topology in  $pp$  reactions. As mentioned before, we employ the event generator PYTHIA v6.2 which has been adjusted with respect to the  $\langle k_\perp^2 \rangle$  parameter to properly describe the

transverse hadron spectra at  $\sqrt{s} = 200$  GeV (cf. Fig. 1 in Ref. [35]). As a trigger particle we choose a charged high  $p_{\perp}$  hadron in the rapidity interval  $|y_{cm}| < 0.5$  with momentum  $4 \text{ GeV}/c \leq p_{\perp}^{Trig} \leq 6 \text{ GeV}/c$  as in Ref. [15]. The correlated particles then are selected in the interval  $2 \text{ GeV}/c \leq p_{\perp}^{Sec} \leq p_{\perp}^{Trig}$  and  $|y_{cm}| < 1.0$ . The resulting angular correlation

$$C(\Delta\varphi) = \frac{1}{N_{Trig}} \frac{dN}{d\Delta\varphi} \quad (2)$$

with respect to the azimuthal angle of the trigger particle is displayed in Fig. 1 (upper left part) and shows two distinct peaks which are attributed to 'near-side' and 'far-side' jet correlations since the maxima at  $\varphi=0$  and  $\varphi=\pi$  correspond to back-to-back emission. Furthermore, the comparison to the data from the STAR Collaboration [15] shows that the angular correlations measured for  $pp$  reactions at  $\sqrt{s} = 200$  GeV are well reproduced by the event generator PYTHIA v6.2.

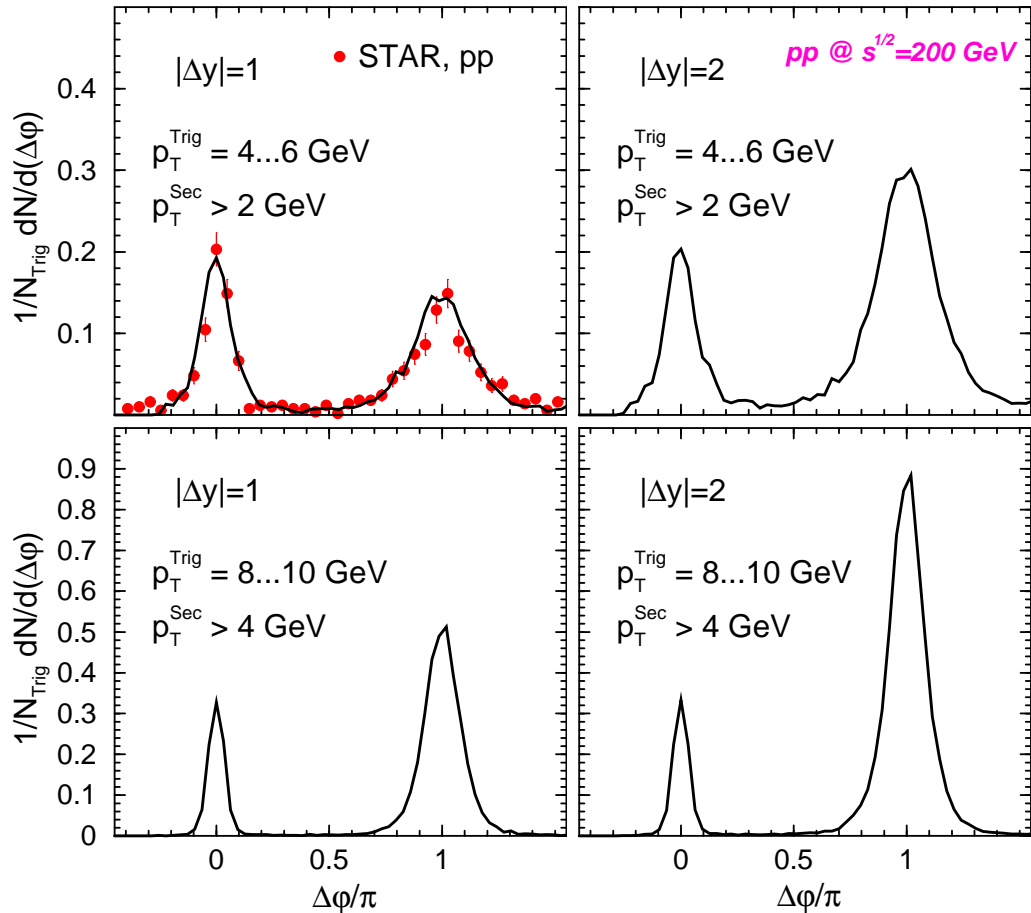


Fig. 1. The correlation in the azimuthal angle  $\varphi$  for  $pp$  reactions at  $\sqrt{s} = 200$  GeV for different cuts on the trigger particle and associated particles from the event generator PYTHIA v6.2. The data in the upper left part are taken from Ref. [15].

The structure and relative height of the two peaks changes when selecting momenta  $8 \text{ GeV}/c \leq p_{\perp}^{Trig} \leq 10 \text{ GeV}/c$  for the trigger particle and  $4 \text{ GeV}/c \leq p_{\perp}^{Sec} \leq p_{\perp}^{Trig}$  for the other charged hadrons (cf. Fig. 1, lower left part). In case of the higher momentum trigger particle the angular distribution of associated hadrons (from jet fragmentation) becomes narrower; the 'far-side' peak gets larger since the number of associated hadrons in the peaks are lower than for the cuts in the upper left part of Fig. 1. The asymmetry in the height of the peaks is due to the fact that the 'trigger particle' is not counted in the 'near-side' angular correlation. Apart from the sensitivity to the momentum cuts demonstrated above the height of the peaks also depends on the rapidity cut for the associated particles. When gating on a larger rapidity interval  $|\Delta y| = 2$  (r.h.s. of Fig. 1) the 'near-side' peak roughly stays the same whereas the 'far-side' peak increases by almost a factor of two.

A more detailed information is provided in the upper part of Table 1 where the probability of finding  $0, 1, \dots, 3$  further hadrons in the 'near-side' and 'far-side' peak is given for  $4 \text{ GeV}/c \leq p_{\perp}^{Trig} \leq 6 \text{ GeV}/c$  and  $2 \text{ GeV}/c \leq p_{\perp}^{Sec} \leq p_{\perp}^{Trig}$  and  $|y_{cm}| < 1.0$ . These numbers demonstrate, that in less than 10% of all events a further particle is found in the given rapidity and  $p_{\perp}$  interval and that the conditional probability to find any further particle roughly decreases by an order of magnitude. These low conditional probabilities should be kept in mind when comparing azimuthal angular correlations from Au+Au collisions (cf. Sections 4 and 5). We note additionally that 'jet structures' only show up after averaging over a large event sample.

It is, furthermore, instructive to have a look at the rapidity distribution of charged particles when gating on a trigger hadron in the rapidity interval  $|y_{cm}| < 0.5$  with momentum  $4 \text{ GeV}/c \leq p_{\perp}^{Trig} \leq 6 \text{ GeV}/c$ . The correlated particles in the 'far-side' peak – selected in the interval  $2 \text{ GeV}/c \leq p_{\perp}^{Sec} \leq p_{\perp}^{Trig}$  – then show a rather wide distribution in rapidity as seen from Fig. 2. Here, the upper solid line corresponds to the correlated charged hadrons in the 'far-side' peak (color: red) whereas the lower solid line corresponds to the correlated charged hadrons in the 'near-side' peak (color: green) which is localized in rapidity around the trigger particle. The dashed lines give the rapidity distribution for the correlated charged hadrons in the 'far-side' (upper dashed line, color: red) and 'near-side' peak (upper dashed line, color: red) which correspond to leading particles, i.e. where the hadron carries at least one of the constituent quarks of the initial protons. Note that in  $pp$  collisions two strings are formed with in total four leading particles. For the momentum cuts adopted the leading particles show up dominantly at  $|y| \approx 4$ , i.e. in the rapidity regime of the projectile/target remnants.

Consequently, the hadrons produced and/or formed by the fragmentation of jets do not occupy a narrow rapidity window close to the trigger hadron but are widespread in rapidity at least in the 'far-side' peak (with even a small

#particles		#particles far side			
near side		0	1	2	3
pp @ 200 GeV					
0		0.89	0.047	0.0060	0.00062
1		0.046	0.0078	0.0020	0.00031
2		0.0026	0.0010	0.00049	0.00012
3		0.00030	0.00013	0.000055	0.000017
central Au+Au @ 200 GeV					
0		0.93	0.024	0.0024	0.00034
1		0.040	0.0033	0.00043	0.000023
2		0.0031	0.00041	0.00016	0.000021
3		0.00040	0.00013	0.0000065	0

Table 1

The conditional probability to find in addition to the trigger particle 0,1,...3 particles in the 'far-side' and 0,1,...3 particles in the 'near-side' peak in  $pp$  (upper part) and central  $Au+Au$  collisions (lower part) at  $\sqrt{s} = 200$  GeV. The trigger conditions are:  $4 \text{ GeV}/c \leq p_{\perp}^{Trig} \leq 6 \text{ GeV}/c$  and  $2 \text{ GeV}/c \leq p_{\perp}^{Sec} \leq p_{\perp}^{Trig}$  and  $|y_{cm}| < 1.0$ .

dip at midrapidity). This wide distribution also explains why the probability of observing a correlated hadron together with a trigger hadron in roughly the same rapidity interval  $|\Delta y| \approx 1$  and high momentum is rather low (cf. upper part of Table 1).

### 3 Ingredients of the transport model

We employ the HSD transport model [38,44,45] for our study of  $p+A$ ,  $d+A$  and  $A+A$  collisions. This approach takes into account the formation and multiple rescattering of formed hadrons as well as unformed 'leading' pre-hadrons and thus incorporates the dominant final state interactions. In the transport approach we include nucleons,  $\Delta$ 's,  $N^*(1440)$ ,  $N^*(1535)$ ,  $\Lambda$ ,  $\Sigma$  and  $\Sigma^*$  hyperons,  $\Xi$ 's,  $\Xi^*$ 's and  $\Omega$ 's as well as their antiparticles on the baryonic side whereas the  $0^-$  and  $1^-$  octet states are included in the mesonic sector. Inelastic hadron-hadron collisions with energies above  $\sqrt{s} \simeq 2.6$  GeV are described by the FRITIOF model [47] (employing PYTHIA v5.5 with JETSET v7.3 for the production and fragmentation of jets [48]) whereas low energy hadron-hadron collisions are modeled in line with experimental cross sections. We mention that no explicit parton cascading is involved in our transport calculations contrary to e.g. the AMPT model [49] or explicit parton cascades [50].

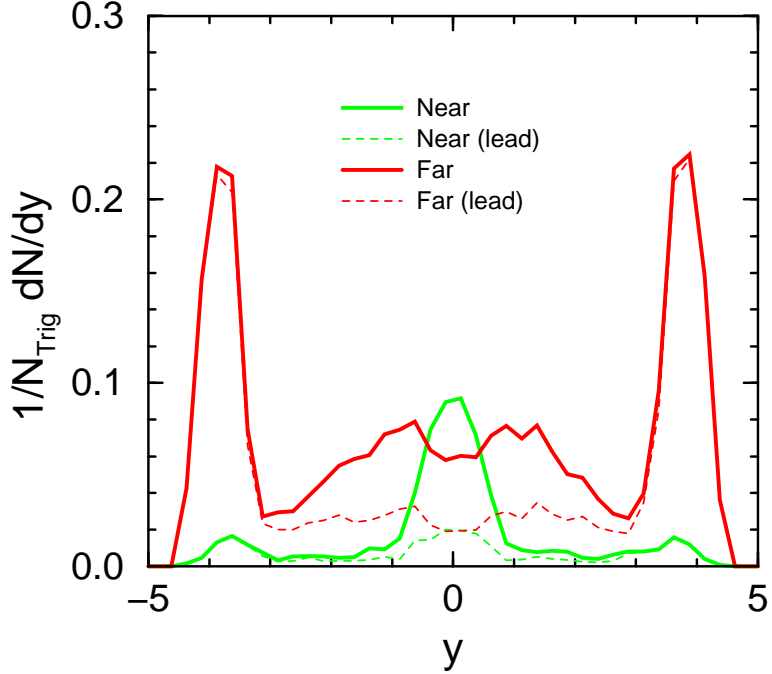


Fig. 2. The rapidity distribution of correlated hadrons when gating on a high  $p_{\perp}^{Trig}$  hadron in the interval  $4 \leq p_{\perp}^{Trig} \leq 6$  GeV/c for  $|y| < 0.5$  and  $2 \leq p_{\perp}^{Sec} \leq p_{\perp}^{Trig}$ . The 'near-side' contribution is also peaked at midrapidity (lower solid line, color: green), however, shows only a small content of 'leading' particles (lower dashed line, color: green). On the other hand, the rapidity distribution of correlated hadrons in the 'far-side' peak (upper solid line, color: red) is widespread with maxima around  $|y| \approx 4$  dominantly due to leading hadrons (upper dashed line, color: red).

A systematic analysis of HSD results and experimental data for central nucleus–nucleus collisions for 2 AGeV to 21.3 ATeV has shown that the spectra for the 'longitudinal' rapidity distribution of protons, pions, kaons, antikaons and hyperons are in reasonable agreement with available data. Only the pion rapidity spectra are slightly overestimated from AGS to SPS energies [51,52,53] which implies, that the maximum in the  $K^+/\pi^+$  ratio at  $20 \cdots 30$  AGeV – seen in central Au+Au (Pb+Pb) collisions [54] – is missed. Furthermore, there are more severe problems with the dynamics in the direction transverse to the beam. Whereas the pion transverse momentum spectra are rather well described from lower AGS to top RHIC energies the transverse momentum slopes of kaons/antikaons are clearly underestimated above  $\sim 5$  AGeV in central Au+Au collisions. In Ref. [53] this failure has been attributed to a lack of pressure generation in the very early phase of the heavy-ion collisions which also points towards a new state of very strongly interacting matter in the very early phase of central Au+Au (or Pb+Pb) collisions. In addition, the elliptic flow of high  $p_{\perp}$  hadrons is missed substantially [35] which also suggests strongly interacting matter in the very early phase.

Inspite of the deficiencies pointed out the overall reproduction of the exper-

imental spectra is sufficiently realistic such that we can proceed with more exclusive probes that are produced and propagated in the background of the expanding string/hadron matter generated in relativistic nucleus-nucleus collisions.

### 3.1 Perturbative treatment of high $p_\perp$ hadrons and jets

For the production and propagation of hadrons with high transverse momentum ( $> 1.5 \text{ GeV}/c$ ) we employ a perturbative scheme as also used in Refs. [2,55] for the charm and open charm degrees of freedom and in Ref. [35] for high  $p_\perp$  hadrons.

The initial conditions for the production and also subsequent propagation of hadrons with moderate to high transverse momentum ( $> 1.5 \text{ GeV}/c$ ) are incorporated in the HSD approach by a superposition of  $pp$  collisions described via PYTHIA [43] which serve as the basic input. The partons (from PYTHIA) fragment to hadrons – according to the JETSET-part of PYTHIA – with the vacuum fragmentation functions. We mention that medium-modified fragmentation schemes might have to be employed for nucleus-nucleus collisions, however, we will only use the vacuum fragmentation functions in this study in order to find out, if this minimal scheme also applies for the heavy-ion case. Together with the 4-momenta of all resulting 'particles' we store the constituent quark content and the relative weight  $W_i$  of each event.

The weight  $W_i$  is given by the ratio of the actual production cross section divided by the inelastic nucleon–nucleon cross section, e.g.

$$W_i = \frac{\sigma_{NN \rightarrow h(p_\perp) + x}(\sqrt{s})}{\sigma_{NN}^{\text{inelas.}}(\sqrt{s})}. \quad (3)$$

All 'particles' with one or more constituent quarks are denoted as 'pre-hadrons' while those without are denoted as 'secondary' hadrons. The pre-hadrons start propagating in space-time from the space-time position of the individual interaction vertex  $x_V^i$ , which is well defined from the transport calculation, and begin to interact immediately with a fractional cross section according to the constituent quark model (see below). The 'secondaries' are inserted in the dynamical calculation after their formation time  $t_f$  (in the actual reference frame) at a space-time position which is displayed from the vertex  $x_V^i$  by  $\mathbf{v}_j \cdot t_f$  with  $\mathbf{v}_j$  denoting the velocity of the 'secondary' hadron  $j$ . The velocity  $\mathbf{v}_j$  is fixed in the calculation by the momentum and energy of the finally formed hadron  $j$ , which is an approximation. In practice the major fraction of 'secondaries' shows up with velocities close to 1 (in units of  $c$ ) such that alternative modelings have no major effect on the final results for attenuation.

We then follow the motion of the perturbative hadrons within the full background of strings/hadrons by propagating them as free particles, i.e. neglecting in-medium potentials, but compute their collisional history with baryons and mesons or quarks and diquarks. For reactions with diquarks we use the corresponding reaction cross section with baryons multiplied by a factor of 2/3. For collisions with quarks (antiquarks) we adopt half of the cross section for collisions with mesons and for the leading pre-hadron (formed) baryon collision a factor of 1/3 is assumed. The elastic and inelastic interactions with their fractional cross section are modeled in the HSD approach in the same way as for ordinary hadrons with the same quantum numbers via the FRITIOF model [47] (including PYTHIA v5.5 with JETSET v7.3 for the production and fragmentation of jets [48]). This concept – oriented along the additive quark model – has been proven to work rather well for nucleus–nucleus collisions from AGS to RHIC energies [51,52,53] as well as in hadron formation and attenuation in deep inelastic lepton scattering off nuclei [39,40]. We stress again that the latter reactions are important to understand the attenuation of pre-hadrons or ordinary hadrons with high momentum in 'cold' nuclear matter [37]. Our studies in Ref. [39,40] have demonstrated that the dominant final state interactions of the hadrons with maximum momentum, as measured by the HERMES collaboration [42], are compatible to the concepts described above. This also holds for antiproton production and attenuation in proton–nucleus collisions at AGS energies [56].

### 3.2 *Simulation of the Cronin effect in $pA$ , $dA$ and $AA$ collisions*

As known from the experimental studies of Refs. [57,58] an enhancement of the high transverse momentum particle cross section from proton–nucleus collisions – relative to scaled  $pp$  collisions – is already observed at SPS and ISR energies. This 'Cronin effect' is probably related to an increase of the average transverse momentum squared  $\langle k_\perp^2 \rangle$  of the partons in the nuclear medium. One may speculate that such an enhancement of  $\langle k_\perp^2 \rangle$  is due to induced initial semi-hard gluon radiation in the medium, which is not present in the vacuum due to color neutrality [25,37]. Since the microscopic mechanisms are beyond the scope of our present analysis, we simulate this effect in the transport approach by increasing the average  $\langle k_\perp^2 \rangle$  in the string fragmentation with the number of previous collisions  $N_{\text{prev}}$  as [35,53,59]

$$\langle k_\perp^2 \rangle = \langle k_\perp^2 \rangle_{pp} (1 + \alpha N_{\text{prev}}) . \quad (4)$$

The parameter  $\alpha \approx 0.25 – 0.4$  in (4) has been fixed in comparison to the experimental data for  $d+Au$  collisions at RHIC [13,14] in Ref. [35]. As discussed in our previous analysis [35] the Cronin effect has an essential impact on the

shape of the nuclear modification factor

$$R_{AA}(p_\perp) = \frac{1/N_{AA}^{\text{event}} d^2N_{AA}/dydp_\perp}{\langle N_{\text{coll}} \rangle / \sigma_{pp}^{\text{inelas}} d^2\sigma_{pp}/dydp_\perp} \quad (5)$$

used experimentally to quantify the in-medium effects from d+Au or A+A collisions relative to  $pp$  reactions. In (5) the quantity  $\langle N_{\text{coll}} \rangle$  denotes the number of binary nucleon-nucleon collisions – directly available from the transport calculation – while  $\sigma_{pp}^{\text{inelas}}$  stands for the inelastic nucleon-nucleon cross section (known experimentally).

#### 4 Results of Transport calculations for Au+Au collisions at $\sqrt{s} = 200$ GeV

We recall that the detailed analysis of high  $p_\perp$  hadron attenuation at the top RHIC energy of  $\sqrt{s} = 200$  GeV in Ref. [35] has demonstrated: i) the (pre-) hadronic final state interactions are able to approximately reproduce the high  $p_\perp$  suppression effects observed in d+Au and Au+Au collisions; ii) the interactions of formed hadrons after a formation time  $t_f \approx 0.8$  fm/c are not able to explain the attenuation observed for transverse momenta  $p_\perp \geq 6$  GeV/c, whereas the shape of the ratio  $R_{AA}$  (5) in transverse momentum  $p_\perp$  reflects the presence of final state interactions of formed hadrons in the 1-4 GeV/c range; iii) the attenuation by (pre-) hadronic final state interactions is insufficient to explain the large suppression seen experimentally in central Au+Au collisions. Since our transport calculations are identical with those presented in [35] we directly continue with the new analysis on jet suppression.

Fig. 3 shows our results for Au+Au collisions at  $\sqrt{s} = 200$  GeV for different centrality classes with respect to the 'near-side' and 'far-side' angular correlation of charged hadrons. We have gated on high  $p_\perp$  particles in the interval ( $p_\perp^{\text{Trig}} = 4 \dots 6$  GeV/c) and accumulated further charged hadrons in the interval  $p_\perp = 2$  GeV  $\dots p_\perp^{\text{Trig}}$  ( $|y| < 0.7$ ). In addition to the angular correlations from Au+Au collisions we have added the results from  $pp$  reactions (dashed lines) in comparison to the data from STAR for  $pp$  collisions [15] (full dots) for each centrality bin to demonstrate both the actual statistical uncertainty due to different event samples for the varying centralities (dashed lines) and the actual attenuation generated by the final state interactions in the transport calculation (solid lines, color: green).

We find that – when gating on high  $p_\perp$  hadrons (in the vacuum) – the 'near-side' correlations are close to the 'near-side' correlations observed for jet fragmentation in the vacuum (cf. lower part of Table 1) for all centralities. This is in agreement with the experimental observation [9,15]. Furthermore, for the

'far-side' correlations we get a  $\sim 60\%$  reduction for the most central collisions but not an almost complete disappearance of the 'far-side' jet as indicated by the experimental data [9,15]. The latter data for central Au+Au collisions are displayed in the upper left part of Fig. 3 by the open squares. The suppression for 5–20 %, 20–45% and 45–65% centralities in the 'far-side' peak is lower than for the 5% most central reactions, but not dramatically different.

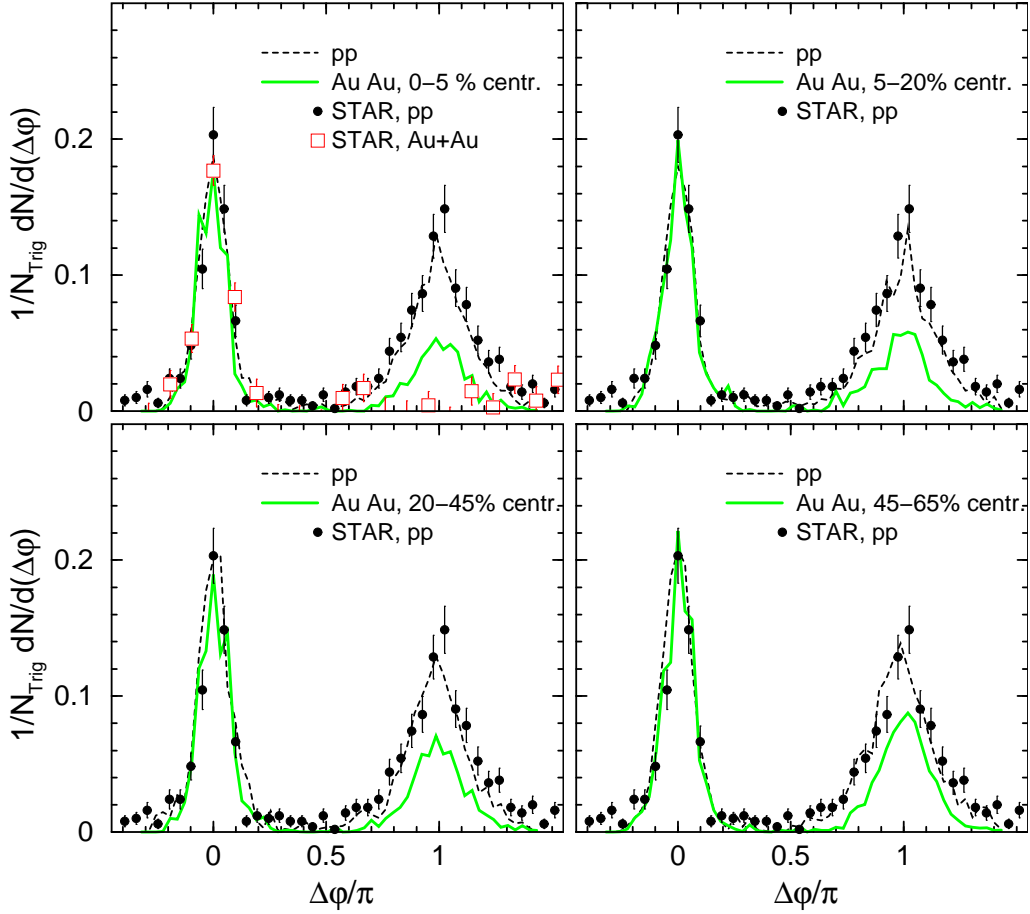


Fig. 3. 'Near-side' and 'far-side' jet-like correlations from HSD for p+p and central Au+Au collisions at midrapidity for  $p_{\perp}^{Trig} = 4 \dots 6 \text{ GeV}/c$  and  $p_{\perp} = 2 \text{ GeV}/c \dots p_{\perp}^{Trig}$  ( $|y| < 0.7$ ) at different centralities. Data for p+p (full dots) are from [15]. The dashed lines show our input to the transport calculations for each centrality class, while the solid lines show the result including the final state interactions (color: green). The experimental data [9,15] for central Au+Au collisions are displayed in the upper left part by the open squares (color: red). Note, however, that the experimental trigger is  $p_{\perp}^{Trig} = 4 \dots 6 \text{ GeV}/c$  and further charged hadrons have been accumulated in the interval  $p_{\perp} = 2 \text{ GeV} \dots p_{\perp}^{Trig}$  for  $|\Delta\eta| < 0.5$  with respect to the trigger particle. Thus the trigger conditions differ slightly from those in the calculations.

In order to become more quantitative, we show in Fig. 4 the integral over the

'far-side' peaks (cf. Fig. 4)

$$I_{AA} = \frac{\int_{\pi/2}^{3\pi/2} d\varphi C(\Delta\varphi)_{AA}}{\int_{\pi/2}^{3\pi/2} d\varphi C(\Delta\varphi)_{pp}} \quad (6)$$

as a function of the number of participating nucleons  $A_{part}$  normalized to the respective integral for  $pp$  reactions. The HSD calculations (full dots) indicate a rather fast drop with  $A_{part}$  and almost become constant for  $A_{part} > 150$ . We note that experimentally the decrease of a very similar ratio appears to continue more strongly with  $A_{part}$  [9] (open squares with error bars in Fig. 4). For orientation the shaded area (color: green) shows an attenuation  $\sim A_{part}^{1/3}$ , where the relative strength has been fixed by either the calculated result at low or high  $A_{part}$ , respectively. Apparently, this power law in  $A_{part}$  is too strong in comparison to the transport calculation (full dots).

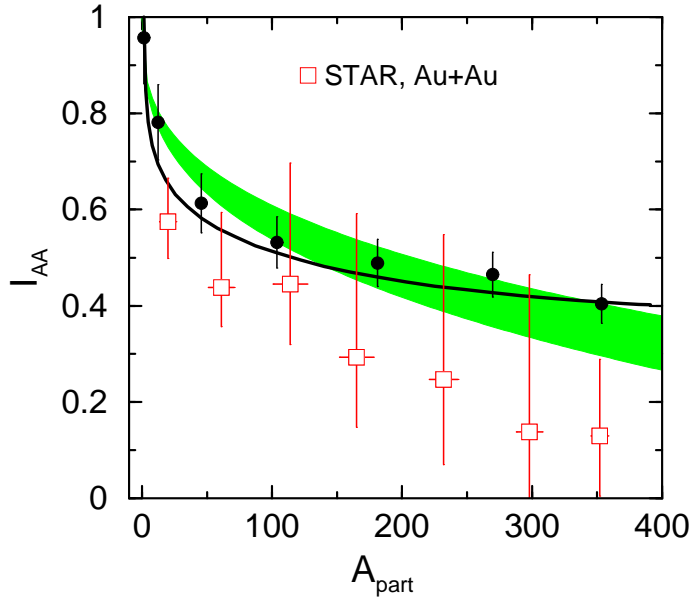


Fig. 4. The angular integral over the 'far-side' correlation (6) for Au+Au at  $\sqrt{s} = 200$  GeV from HSD (full dots with statistical error bars) as a function of the number of participating nucleons  $A_{part}$ . The shaded area shows an attenuation  $\sim A_{part}^{1/3}$ , where the relative strength has been fixed by the calculated result either at low or high  $A_{part}$ , respectively. The solid line results from the simple estimate (7) when plotted versus  $A_{part}$  and fixed in size at high  $A_{part}$ . The experimental data [9] are displayed in terms of the open squares (color: red) where the statistical and systematic errors have been added quadratically. Note, however, that experimentally the associated charged hadrons have been accumulated in the interval  $p_{\perp} = 2 \text{ GeV} \dots p_{\perp}^{Trig}$  for  $|\Delta\eta| < 0.5$  with respect to the trigger particle. Furthermore, the angular integrations have been carried out in a slightly larger angular range.

We note that a rather good reproduction of the HSD results is obtained when comparing to the quadratic average of the long and short axis of the almond

shaped interaction zone – in  $x, y$  direction – as a function of impact parameter  $b$ ,

$$L(b) = \frac{1}{2} \sqrt{R_L^2 + R_S^2} \quad (7)$$

with  $R_L = \sqrt{R^2 - b^2/4}$ ,  $R_S = R - b/2$  and  $R$  denoting the radius of the Au-target in hard-sphere geometry. The resulting suppression is displayed in terms of the solid line in Fig. 4 – fixed in absolute magnitude at high  $A_{part}$  – using the relation  $A_{part}(b)$ . In view of the agreement between the rough estimate (7) and the numerical results of the HSD calculations we conclude that the suppression in the transport calculations is essentially determined by a linear geometrical length scale, i.e. by the average jet propagation length in the almond shaped reaction zone (cf. Ref. [60]). Note in addition that the relation  $A_{part}(b)$  is model dependent for very peripheral reactions (small  $A_{part}$ ).

Since the suppression of 'far-side' jets from pre-hadronic final state interactions in our transport calculations is less than 60% at all centralities, there should be an additional suppression mechanism at least for mid-central and central collisions that is not included in the present transport approach. Since the dynamics at intermediate and late times are expected to be properly described by HSD only the very early phase of the nucleus-nucleus collision should be failed.

We recall that in HSD (as well as UrQMD [3,4]) there are dominantly collisions of pre-hadrons (string ends) in the early collision phase which neither generate enough early transverse pressure [53], elliptic flow [52,61,62] or attenuation of high  $p_\perp$  hadrons [35,36]. These general findings are in line with those seen in the suppression of 'far-side' jets in Figs. 3 and 4: the medium of strings (pre-hadrons) is not interacting strongly enough to explain an almost complete quenching of 'far-side' jets in central Au+Au collisions at  $\sqrt{s} = 200$  GeV. Nevertheless, about 60% (in central Au+Au collisions) is still a considerable amount of attenuation that should be missed in parton scenarios based on perturbative QCD cross sections.

As mentioned before the hadron formation time  $\tau_f$  is a sensible parameter of the transport approach although fixed by hadron rapidity distributions [38]. Nevertheless, one might argue that this formation time is simply not short enough and an alternative 'fixing' might yield the proper jet suppression. A similar analysis e.g. has been performed in Ref. [62] with respect to the strength of the elliptic flow  $v_2$  of charged hadrons, where shorter formation times  $\tau_f$  lead to an increase of the interaction rate at short times and consequently to a rise of the elliptic flow. To this aim we have performed calculations for 5% central Au+Au collisions at  $\sqrt{s} = 200$  GeV introducing an independent formation time  $\tau_f$  for the jets and their fragmentation products without

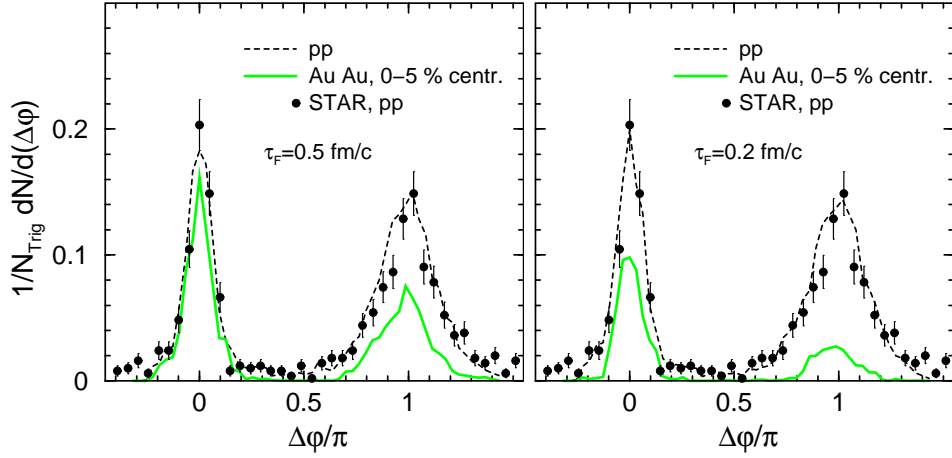


Fig. 5. The same as in Fig. 3 for most central collisions (upper left part), but now for formation times  $\tau_f = 0.5$  fm/c (l.h.s.) and  $0.2$  fm/c (r.h.s.) instead of the default value of  $0.8$  fm/c in Fig. 3.

changing the formation time of the bulk 'non-perturbative' hadrons. The results of these calculations for the azimuthal angular correlations are shown in Fig. 5 for  $\tau_f = 0.5$  (l.h.s.) and  $0.2$  fm/c (r.h.s.) by the solid lines (color: green). In fact, the attenuation of the 'far-side' peak increases with decreasing formation time. However, also the 'near-side' peak now shows a reduction by the final state interactions as seen from a comparison of the dashed and solid lines. This reduction of the 'near-side' peak is still very modest for  $\tau_f = 0.5$  fm/c but reaches a level of  $\sim 50\%$  for  $\tau_f = 0.2$  fm/c which can clearly be ruled out by the present data. In short: a sizeable reduction of the formation time - though leading to a more substantial suppression of the 'far-side' peak as well as to an increase of the elliptic flow of charged hadrons [34,62] - is incompatible with the experimental observations for central Au+Au collisions.

Without explicit representation we mention that a decrease in the energy density cut for hadron formation (cf. Ref. [35]) from  $1$  GeV/fm $^3$  to  $0.7$  GeV/fm $^3$  leads only to a small reduction of the 'far-side' jet suppression. This also holds for a moderate increase of the cross section for the pre-hadronic states. These results are easy to understand: The 'leading' pre-hadrons in central collisions are attenuated by a factor of about 15 (cf. Fig. 8 of [35]) with the standard cross sections, such that these particles are practically erased. Furthermore, only 70-80% of high  $p_\perp$  hadrons are pre-hadrons (cf. Fig. 3 in [35]). We point out that a larger cross section would violate unitarity since the full hadronic cross section for short time scales is already exploited within the constituent quark model. Accordingly, the 'secondaries' have to start with a vanishing cross section at the space-time point of the vertex or more precisely starting from the quark-antiquark production point that we denote by  $t_p$  (cf. Fig. 3 in [39]) which is a fraction of  $1$  fm/c. During the early times, when the system is very dense, the 'secondaries' thus have small or vanishing cross section up to their hadron formation time  $\tau_f$  (1). The latter becomes large for high  $p_\perp$  mo-

menta such that the attenuation of 'secondaries' is rather low when employing high  $p_{\perp}$  cuts.

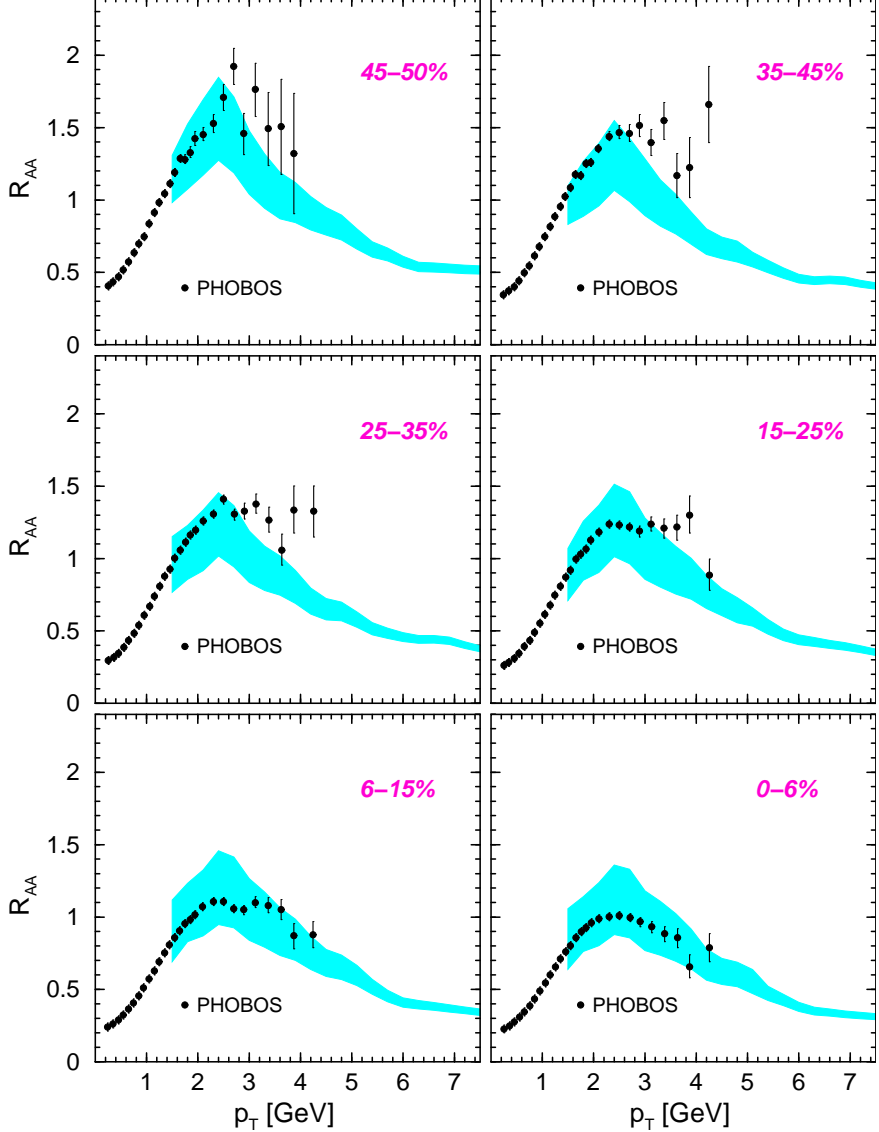


Fig. 6. The ratio  $R_{AA}$  (5) of charged hadrons for different centralities for Au+Au at  $\sqrt{s} = 62.4$  GeV. The experimental data are from Ref. [46]. The hatched bands correspond to our calculations with a Cronin parameter  $\alpha$  in (4) ranging from 0.25 to 0.4 as in Ref. [35].

## 5 Au+Au collisions at $\sqrt{s} = 62.4$ GeV

The system Au+Au at  $\sqrt{s} = 62.4$  GeV has recently been investigated experimentally at RHIC and first results on hadron attenuation have become available at moderate  $p_{\perp}$  from the PHOBOS Collaboration [46]. We thus start

with single hadron attenuation in the next subsection following exactly the studies in Ref. [35] that have been performed at  $\sqrt{s} = 200$  GeV. Since all details have been presented in the former publication we step on with the actual results. However, it is worth to point out that the 'Cronin enhancement factors' are higher at  $\sqrt{s} = 62.4$  GeV than at  $\sqrt{s} = 200$  GeV due to steeper hadron spectra in  $p_\perp$  (cf. also Ref. [30]).

### 5.1 High $p_\perp$ hadron suppression

The centrality dependence of the ratio  $R_{AA}$  for charged hadrons is shown in Fig. 6 for 0 %  $\dots$  6 %, 6 %  $\dots$  15 %, 15 %  $\dots$  25 %, 25 %  $\dots$  35 %, 35 %  $\dots$  45 % and 45 %  $\dots$  50 % centrality of Au+Au collisions at  $\sqrt{s} = 62$  GeV. Again the hatched bands (color: light blue) correspond to our calculations with a Cronin parameter  $\alpha$  in (4) ranging from 0.25 to 0.4 while the data stem from Ref. [46]. Note, that the uncertainty in the Cronin enhancement (width of the hatched band) decreases slightly for more peripheral reactions, which is a direct consequence of the lower number of hard  $NN$  collisions in (4).

We emphasize, that the Cronin enhancement is most visible at momenta up to 5 GeV/c but is practically negligible for  $p_\perp > 6\text{--}8$  GeV/c. As pointed out before in Ref. [35], the suppression seen in the calculation for larger transverse momentum hadrons is due to the interactions of the leading (pre-)hadrons with target/projectile nucleons and the bulk of low momentum hadrons. Accordingly, the ratio  $R_{AA}$  drops below 1 in Fig. 6 in the high momentum regime reaching an attenuation which is about the same as that in the calculations for  $\sqrt{s} = 200$  GeV and  $p_\perp > 5$  GeV/c. Our numerical results in Fig. 6 are roughly compatible with the data from the PHOBOS Collaboration [46] but measurements at higher transverse momenta will be necessary to prove/disprove the dropping of the ratio  $R_{AA}$  with momentum  $p_\perp$  (cf. also Ref. [63]).

### 5.2 Jet correlations from $pp$ and Au+Au collisions

Whereas first experimental information on the single hadron attenuation is available (cf. previous subsection) the quenching of 'far-side' jets at  $\sqrt{s} = 62.4$  GeV is still unknown from the experimental side. In this respect we provide predictions on the basis of our HSD calculations for the angular correlations in  $pp$  and Au+Au collisions.

In Fig. 7 we show the angular correlations of 'near-side' and 'far-side' charged hadrons by gating on high  $p_\perp$  particles in the interval ( $p_\perp^{Trig} = 3 \dots 6$  GeV/c) and accumulating further charged hadrons in the interval  $p_\perp = 2$  GeV  $\dots$   $p_\perp^{Trig}$  ( $|y| < 1.0$ ). In addition to the angular correlations from central Au+Au colli-

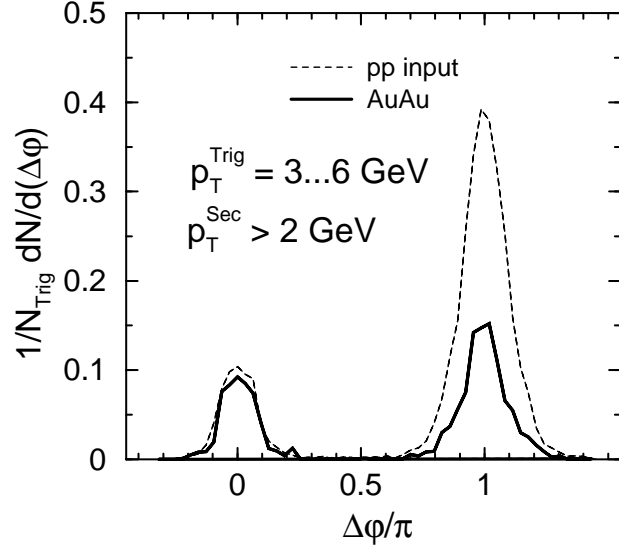


Fig. 7. 'Near-side' and 'far-side' jet-like correlations from HSD for p+p (dashed lines) and central Au+Au collisions (solid lines) at midrapidity for  $p_{\perp}^{Trig} = 3 \dots 6 \text{ GeV}/c$  with  $p_{\perp} = 2 \text{ GeV}/c \dots p_{\perp}^{Trig}$  at  $\sqrt{s} = 62.4 \text{ GeV}$ .

sions (solid lines) we have added the results from  $pp$  reactions (dashed lines) as resulting from the PYTHIA calculations. These PYTHIA results serve again as reference lines for the angular correlation without any final state interaction.

It is seen from the  $pp$  as well as Au+Au angular correlations that the 'far-side' peaks are more pronounced (within the cuts taken) than the 'near-side' peaks. This effect can be traced back to the low probability of observing a further hadron close to the 'near-side' peak when gating on a high momentum trigger particle; most of the associated hadrons can be found in the 'far-side' peak. This comes about because the trigger particle is not counted in the 'near-side' correlation whereas the 'far-side' correlation includes the leading particle of the partner jet. This explanation is quantified in Table 2 where the probability for having 0 ... 3 further charged particles in the 'near-side' and 'far-side' region is given for  $pp$  (upper part) and central Au+Au collisions at  $\sqrt{s} = 62.4 \text{ GeV}$ .

The relative suppression of the 'near-side' peak is very moderate whereas the relative suppression of the 'far-side' correlation in central Au+Au relative to  $pp$  reactions is  $\sim 60 \%$  as for  $\sqrt{s} = 200 \text{ GeV}$ . This is basically due to the fact that the cross section of pre-hadrons with ordinary hadrons or quark-diquark fragments of the initial hadrons is almost independent on energy and the string density only moderately lower at  $\sqrt{s} = 62.4 \text{ GeV}$ . On the other hand, ordinary hadrons are allowed to form slightly earlier because the energy density (in the local rest frame) drops faster below  $1 \text{ GeV}/\text{fm}^3$ .

#particles near side	#particles far side			
	0	1	2	3
pp @ 62.4 GeV				
0	0.82	0.13	0.014	0.00062
1	0.026	0.011	0.0032	0.00029
2	0.00068	0.00061	0.00017	0.000041
3	0.000022	0.000007	0.000023	0.0000028
central Au+Au @ 62 GeV				
0	0.91	0.051	0.0036	0.00011
1	0.026	0.0038	0.00061	0.000014
2	0.00033	0.000017	0.000013	0
3	0	0	0	0

Table 2

The conditional probability to find in addition to the trigger particle 0,1,...3 particles at the far side and 0,1,...3 particles at the near side in p+p and central Au+Au collisions at  $\sqrt{s} = 62$  GeV. The trigger conditions are ( $p_{\perp}^{Trig} = 3 \dots 6$  GeV/c) and  $p_{\perp} = 2$  GeV ...  $p_{\perp}^{Trig}$  ( $|y| < 1.0$ ) for the associated hadrons.

## 6 Summary

Summarizing, we point out that (pre-) hadronic final state interactions contribute significantly to the high  $p_{\perp}$  suppression effects observed in Au+Au collisions at RHIC. This finding is important, since the same dynamics also describe the hadron formation and attenuation in deep-inelastic lepton scattering off nuclei at HERMES [39,40] appreciably well. In particular, it has been demonstrated that the centrality dependence of the modification factor  $R_{AA}$  (5) in Au+Au collisions at  $\sqrt{s} = 200$  GeV is well described for peripheral and mid-central collisions on the basis of leading pre-hadron interactions [35] whereas the attenuation in central Au+Au collisions is noticeably underestimated. A similar observation also holds for an analysis of the 'far-side' angular correlations, which show a substantial, but not fully complete suppression in central collisions as indicated by the experimental data [9]. From these results one should conclude that there are some additional (and earlier) interactions of partons in a possibly colored medium that have not been accounted for in our present HSD transport studies.

We have, furthermore, explored the possibility if shorter formations times  $\tau_f$  for the hadrons might lead to an improved description of the angular correlation data since smaller  $\tau_f$  lead to an increase of the interaction rate at early times and to an increase of the elliptic flow of charged hadrons [34,62].

However, for formation times  $\tau_f \leq 0.5$  fm/c also the 'near-side' peak shows a reduction by the final state interactions. This reduction of the 'near-side' peak is still very modest for  $\tau_f = 0.5$  fm/c but reaches a level of  $\sim 50\%$  for  $\tau_f = 0.2$  fm/c which can be ruled out by the present data. In short: a sizeable reduction of the formation time - though leading to a more substantial suppression of the 'far-side' peak and to an increase of the elliptic flow  $v_2$  of hadrons – is incompatible with the experimental observations for central Au+Au collisions.

We close in pointing out that further experimental studies on the suppression of high momentum hadrons from d+Au and Au+Au collisions down to  $\sqrt{s} = 20$  GeV will be necessary to clearly separate initial state Cronin effects from final state attenuation and to disentangle the role of partons in a colored partonic medium from those of interacting pre-hadrons in an approximately color-neutral hot and dense fireball. A major problem, however, is that the jets escaping the medium stem from the corona of the fireball [30,31,60,64] and thus do not carry much information from the dense medium. Nevertheless, 'far-side' jet suppression appears to be a promising observable since the pre-hadronic (color neutral) interactions employed so far lead to a suppression that is dominantly characterized by a linear length scale (cf. the comparison in Fig. 4). Thus when gating on peripheral reactions with  $A_{part}$  from 50 to 150 one might exploit the geometry of the fireball – which is of approximate almond shape – in more detail. To this aim narrow bins in  $A_{part}$  should be performed and the di-hadron correlations be investigated as a function of the azimuthal angle  $\phi$  of the trigger hadron relative to the reaction plane. Furthermore, also several cuts in the minimum transverse momentum of the associated particles should be taken. It is clear that very high statistics for jet correlations will be needed to obtain a solid information. Some experimental work along this direction is presently carried out.

The authors like to acknowledge stimulating discussions with C. Greiner, T. Falter, B. Kopeliovich and I. Vitev throughout this study.

## References

- [1] J.D. Bjorken, Phys. Rev. D 27 (1983) 140.
- [2] W. Cassing and C. M. Ko, Phys. Lett. B 396 (1997) 39.
- [3] S.A. Bass *et al.*, Prog. Part. Nucl. Phys. 42 (1998) 279.
- [4] M. Bleicher *et al.*, J. Phys. G 25 (1999) 1859.
- [5] F. Karsch *et al.*, Nucl. Phys. B 502 (2001) 321.

- [6] Quark Matter '02, Nucl. Phys. A 715 (2003) 1; Quark Matter '04, J. Phys. G 30 (2004) S633 *ff.*
- [7] J. L. Nagle and T. S. Ullrich, nucl-ex/0203007.
- [8] M. Gyulassy and L. McLerran, nucl-th/0405013.
- [9] C. Adler *et al.* [STAR], Phys. Rev. Lett. 90 (2003) 082302.
- [10] S. S. Adler *et al.* [PHENIX], Phys. Rev. C 69 (2004) 034910.
- [11] J. Adams *et al.* [STAR], Phys. Rev. Lett. 91 (2003) 172302.
- [12] I. Arsene *et al.* [BRAHMS], Phys. Rev. Lett. 91 (2003) 072305.
- [13] S. S. Adler *et al.* [PHENIX], Phys. Rev. Lett. 91 (2003) 072303.
- [14] J. Adams *et al.* [STAR], Phys. Rev. Lett. 91 (2003) 072304.
- [15] C. Adler *et al.*, [STAR], Phys. Rev. Lett. 90 (2003) 082302.
- [16] J. Adams et al., [STAR], nucl-ex/0407007.
- [17] A. H. Tang *et al.*, [STAR], J. Phys. G 30 (2004) S1235.
- [18] M. Gyulassy and M. Plumer, Phys. Lett. B 243 (1990) 432.
- [19] X.-N. Wang and M. Gyulassy, Phys. Rev. Lett. 68 (1992) 1480.
- [20] X. N. Wang, Phys. Rev. C 58 (1998) 2321.
- [21] R. Baier *et al.*, Ann. Rev. Nucl. Part. Sci. 50 (2000) 37.
- [22] M. Gyulassy, I. Vitev, X. N. Wang, and B. Zhang, nucl-th/0302077, in 'Quark Gluon Plasma 3', eds. R. C. Hwa and X.-N. Wang, World Scientific, Singapore 2004.
- [23] X. N. Wang, Phys. Rev. C 61 (2000) 064910.
- [24] Y. Zhang *et al.*, Phys. Rev. C65 (2002) 034903.
- [25] B. Z. Kopeliovich *et al.*, Phys. Rev. Lett. 88 (2002) 232303.
- [26] A. Accardi, hep-ph/0212148; A. Accardi and M. Gyulassy, J. Phys. G 30 (2004) S969.
- [27] I. Vitev, Phys. Lett. B562 (2003) 36; J. Phys. G 30 (2004) S791.
- [28] D. Kharzeev, E. Levin, and L. McLerran, Phys. Lett. B 561 (2003) 93.
- [29] X.-N. Wang, Phys. Lett. B 579 (2004) 299.
- [30] A. Dainese, C. Loizides, and G. Paic, hep-ph/0406201.
- [31] K. J. Eskola, H. Honkanen, C. A. Salgado, and U. A. Wiedemann, hep-ph/0406319.

- [32] K. Gallmeister, C. Greiner, and Z. Xu, Phys. Rev. C 67 (2003) 044905.
- [33] D. E. Kahana and S. H. Kahana, nucl-th/0406074.
- [34] D. Hardtke and T. J. Humanic, nucl-th/0405064.
- [35] W. Cassing, K. Gallmeister, and C. Greiner, Nucl. Phys. A 735 (2004) 277.
- [36] W. Cassing, K. Gallmeister, and C. Greiner, J. Phys. G 30 (2004) S801.
- [37] B. Z. Kopeliovich, J. Nemchick, E. Predazzi, and A. Hayashigaki, Nucl. Phys. A 740 (2004) 211.
- [38] W. Ehehalt and W. Cassing, Nucl. Phys. A 602 (1996) 449.
- [39] T. Falter, W. Cassing, K. Gallmeister, and U. Mosel., nucl-th/0406023, Phys. Rev. C, in print.
- [40] T. Falter, W. Cassing, K. Gallmeister, and U. Mosel., Phys. Lett. B 594 (2004) 61.
- [41] B. Z. Kopeliovich, Phys. Rev. C 68 (2003) 044906.
- [42] A. Airapetian *et al.* [HERMES], Eur. Phys. J C21 (2001) 599; Phys. Lett. B 577 (2003) 37; P. Di Nezza *et al.* [HERMES], J. Phys. G 30 (2004) S783.
- [43] T. Sjöstrand *et al.*, Comp. Phys. Commun. 135 (2001) 238.
- [44] J. Geiss, W. Cassing, and C. Greiner, Nucl. Phys. A 644 (1998) 107.
- [45] W. Cassing and E. L. Bratkovskaya, Phys. Rep. 308 (1999) 65 .
- [46] B. B. Back *et al.*, [PHOBOS], nucl-ex/0405003.
- [47] H. Pi, Comp. Phys. Commun. 71 (1992) 173.
- [48] H.-U. Bengtsson and T. Sjöstrand, Comp. Phys. Commun. 46 (1987) 43.
- [49] Z. W. Lin *et al.*, Nucl. Phys. A 698 (2002) 375.
- [50] S. A. Bass, B. Müller, and D. K. Srivastava, J. Phys. G 30 (2004) S1283.
- [51] H. Weber, E. L. Bratkovskaya, W. Cassing, and H. Stöcker, Phys. Rev. C 67 (2003) 014904.
- [52] E. L. Bratkovskaya, W. Cassing, and H. Stöcker, Phys. Rev. C 67 (2003) 054905.
- [53] E. L. Bratkovskaya *et al.*, Phys. Rev. C 69 (2004) 054907.
- [54] V. Friese *et al.*, NA49 Collaboration, J. Phys. G 30 (2004) S119.
- [55] W. Cassing, E. L. Bratkovskaya, and A. Sibirtsev, Nucl. Phys. A 691 (2001) 753.
- [56] W. Cassing, E. L. Bratkovskaya, and O. Hansen, Nucl. Phys. A 707 (2002) 224.

- [57] J. W. Cronin *et al.*, Phys. Rev. D 11 (1975) 3105.
- [58] D. Antreasyan *et al.*, Phys. Rev. D 19 (1979) 764.
- [59] G. G. Barnaföldi, G. Papp, P. Levai, and G. Fai, nucl-th/0307062; J. Phys. G 30 (2004) S1125.
- [60] A. Drees, H. Feng, and J. Jia, nucl-th/0310044.
- [61] H. Stöcker, nucl-th/0406018.
- [62] M. Bleicher and H. Stöcker, Phys. Lett. B 526 (2002) 309.
- [63] A. Adil and M. Gyulassy, nucl-th/0405036, Phys. Lett. B, in print.
- [64] B. Müller, Phys. Rev. C 67 (2003) 061901.